Hygro-Thermo-Mechanical Reliability Assessment of a Thermal Interface Material for a Ball Grid Array Package Assembly

Xi Liu
Computer Aided Simulation for Packaging Reliability (CASPaR) Laboratory,
George W. Woodruff School of Mechanical Engineering,
Georgia Institute of Technology,
Atlanta, GA 30332-0405
e-mail: xi.liu@gatech.edu

Jiantao Zheng
IBM Server and Technology Group,
Hopewell Junction, NY 12533
e-mail: jzheng@us.ibm.com

Suresh K. Sitaraman
Computer Aided Simulation for Packaging Reliability (CASPaR) Laboratory,
George W. Woodruff School of Mechanical Engineering,
Georgia Institute of Technology,
Atlanta, GA 30332-0405
e-mail: suresh.sitaraman@me.gatech.edu

The thermal efficacy of thermal interface material (TIM) is highly dependent on its ability to adhere to the surfaces of interest. Any delamination of the TIM from the die or the lid will increase the local thermal resistance and, thus, will reduce the overall effectiveness of the TIM. Although significant amount of work has been done on understanding the thermal and moisture effects of various polymer materials used in microelectronic package assemblies, very limited work has been done to study the effect of temperature and moisture on TIM delamination. In this paper, a sequential hygro-thermal-mechanical finite-element model has been developed to mimic the loadsteps associated with package assembly as well as moisture soaking under 85°C/85RH over 500 h. The predictions from the models have been validated with a wide range of experimental data including laser Moiré data for thermomechanical loading and digital image correlation data for hygro-thermo-mechanical loading. Weight gain and coordinate-measurement machine have been used to characterize moisture diffusivity and moisture expansion coefficient of various polymer materials in the package assembly. The developed models show the evolution of normal strain in TIM during various loadsteps and provide important insight into the potential for TIM delamination under package assembly process and moisture soaking. Thus, the models can be used for developing various designs and process steps for reducing the chances for TIM delamination. [DOI: 10.1115/1.4001746]

Keywords: thermal interface material, debonding, reliability, hygro-thermo-mechanical model

1 Introduction

Moisture sensitivity of electronic package has been of a great concern in the electronic industry for decades. Significant work [1–12] has been done on moisture material property characterization, moisture absorption and desorption analysis, moisture/temperature experimental testing, and their effect on package reliability. Good amount of work has also focused on the effect of moisture during solder reflow [1–3], where "popcorn" failure may occur due to the vaporization of moisture at the interfaces, creating an overpressure condition. Thus, interfacial cracks may initiate and propagate to the edges, providing path for outer corrosive material and further degrade package reliability. Besides, the differential swelling between polymeric and nonpolymeric materials induces hygroscopic strain and stress into the package, which can be the same order of magnitude as thermally induced stress. This is even more serious for flip chip packages than that of wire bonded packages [6–8].

Based on the review of literature, it is seen that less work has been done on the coupled hygrothermal effect on package reliability and even less work has been done on the hygrothermal effect on thermal interface material (TIM) behavior during package assembly and operating conditions.

Thus, the objective of this paper is to develop a fully coupled hygro-thermo-mechanical sequential finite-element (FE) model to study the temperature and moisture effect on TIM behavior during package assembly and reliability testing, including underfilling, lid attach, and gall grid array (BGA) reflow followed by 500 h 85°C/85RH soaking. The developed models have been validated through various experimental data. Furthermore, the validated models can be used to perform parametric analysis to develop package design guidelines.

2 Finite-Element Modeling

In this paper, the moisture diffusion analysis is carried out by moisture-temperature analogy based on the fact that moisture diffusion can be described by Fick's diffusion equation.

$$\frac{\partial C}{\partial t} - \nabla[D \nabla C] = 0 \tag{1}$$

where C is the moisture concentration and D is the diffusivity, which is similar to heat equation, providing the probability to solve moisture diffusion problem using the heat transfer analysis module in ANSYS. The only problem with the direct analogy between temperature T and moisture concentration C is that the temperature T is continuous at the interfaces between different materials while the moisture concentration is not due to the fact that different materials normally have different saturated moisture concentration C_{sat}. To address the moisture concentration continuity issue across material interfaces, another variable, wetness w, was proposed by Wong and co-workers [7,8].

$$w = C/C_{sat} \tag{2}$$

Contributed by the Electronic and Photonic Packaging Division of ASME for publication in the JOURNAL OF ELECTRONIC PACKAGING. Manuscript received January 21, 2010; final manuscript received May 6, 2010; published online June 11, 2010. Assoc. Editor: Giulio Lorenzini.

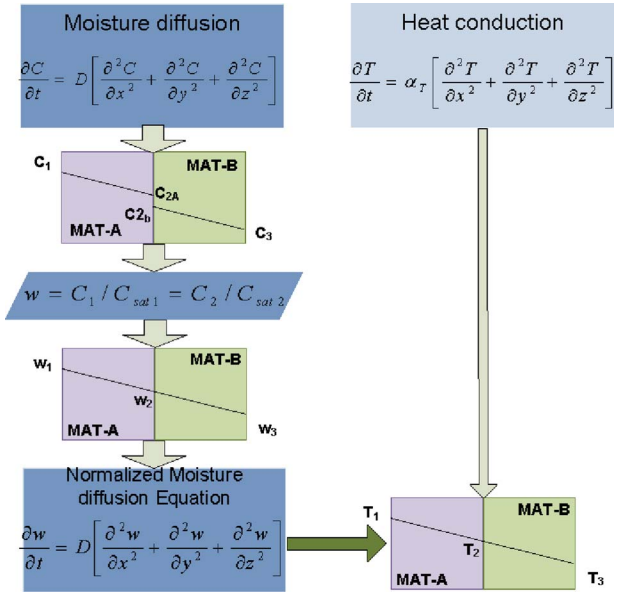

Fig. 1 Wetness and temperature analogy

This new variable, wetness w, has been shown to be continuous across the interface by applying interfacial chemical equilibrium law. With this new variable, the diffusion Eq. (1) becomes

$$\frac{\partial(w \cdot C_{\text{sat}})}{\partial t} - \nabla[D\,\nabla\,(w \cdot C_{\text{sat}})] = 0 \tag{3}$$

For isotropic materials and under constant humidity and temperature experimental conditions, C_{sat} and D are constant and, therefore, Eq. (3) can be rewritten as

$$\frac{\partial^2 w}{\partial x^2} + \frac{\partial^2 w}{\partial y^2} + \frac{\partial^2 w}{\partial z^2} = \frac{1}{D}\frac{\partial w}{\partial t} \tag{4}$$

Equation (4) can be solved using the heat conduction analogy, as illustrated in Fig. 1. As seen in Fig. 2, temperature and wetness are analogous while moisture diffusivity D and thermal diffusivity alpha $(K/\rho c)$ are analogous.

However, since laminates and board, which have very complicated structures, are not isotropic, "effective hygromechanical material properties" are applied based on their weight gain test data.

As shown in Fig. 2, the weight gain data indicates that the diffusivity ($\boldsymbol{D}$) of the laminates is not a constant during the moisture soaking. The Fickian diffusion can only capture the early stage of moisture absorption (first 120 h). Therefore, concentration dependent diffusivities were applied in this model to simulate the non-Fickian behavior, as the pink curve shown in Fig. 2. Details of the curve fitting process please refer to Ref. [13].

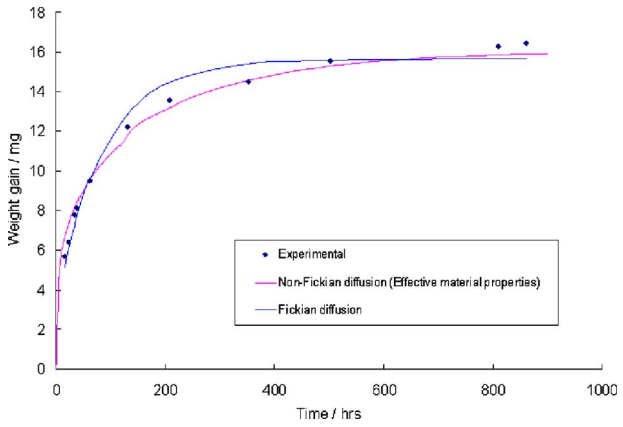

Fig. 2 Weight gain of laminates under 85°C/85RH

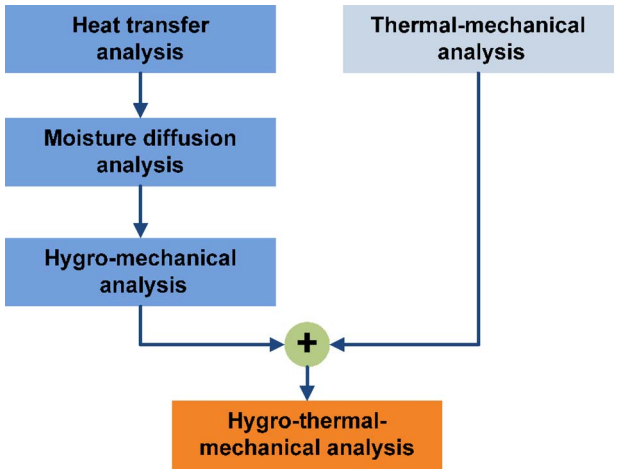

Fig. 3 Flow chart of coupled hygro-thermal-mechanical analysis

The multifield coupling method for hygro-thermal-mechanical analysis is depicted in Fig. 3.

In this work, a sequential three-dimensional quarter-symmetry FE model was built to simulate the package assembly process. The modeled package is shown in Fig. 4, which includes Cu-lid, TIM, chip, first-level solder bumps, underfill, sealband, laminated substrate, second-level ball grid array solder balls, and printed circuit board (PCB). The Cu-lid was modeled as isotropic and elastic, the sealband and TIM were modeled isotropic and thermo-elastic, the laminated substrate and the PCB were modeled with individual layers as thermo-elastic and, thus, the entire substrate or PCB structure as orthotropic, and the BGA solder balls as visco-plastic. As the focus of this paper is on the TIM behavior, the solder bump and underfill interface was modeled using smeared underfill and solder bump thermomechanical properties. Thus, the underfill and solder bump layer was modeled thermo-elastic and orthotropic. For proprietary reasons, the exact values for these properties are not shown here. However, the properties are similar to the ones found in open literature for these commonly used materials.

To capture the process-induced stresses in the package assembly, the thermal profile during the assembly process was applied on the package on a sequential basis. As part of this, starting with a flip chip, underfill, and laminates, the package structure was subjected to underfill cure temperature and cooled down to room temperature. During this simulation, all other components in the package assembly were deactivated using the element birth and death feature available in ANSYS. Subsequently, Cu-lid, TIM, and sealband components were activated, thermal curing and cool down of TIM, and sealband were simulated as illustrated in load-

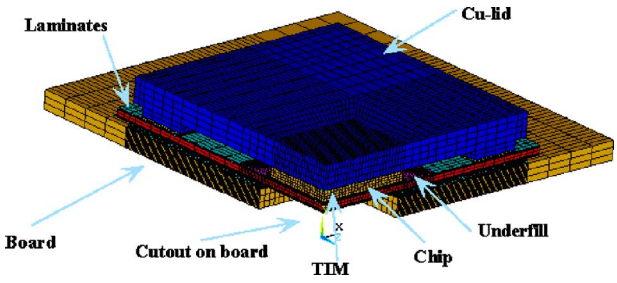

Fig. 4 FE model for hygro-thermal-mechanical analysis

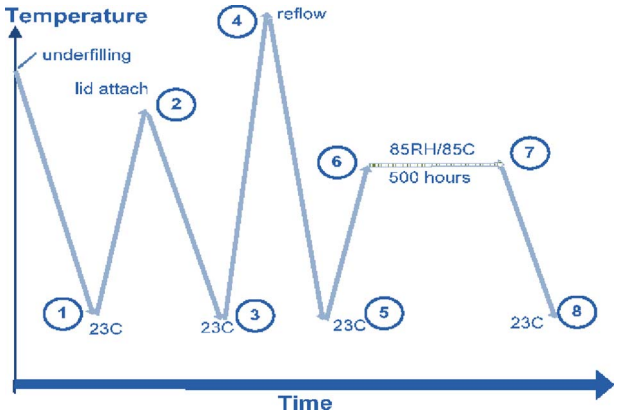

Fig. 5 Loading steps

steps 2 and 3 in Fig. 5. When Cu-lid, TIM, and sealband were activated at loadstep 2, they were assumed to be stress-free at the cure temperature of TIM and sealband. In loadstep 4, the BGA solder balls and PCB were activated and the entire package assembly was cooled down to room temperature at loadstep 5. Thus, at the end of loadstep 5, the thermomechanical stress history of the assembly process has been captured without taking into consideration any of the humidity-related effects. During loadstep 6, the entire assembly is heated to 85°C and the current stress state of the assembly is captured.

In a separate analysis, moisture distribution in the package assembly with 85 RH over 500 h was obtained using the wetness-temperature analogy described earlier. For this purpose, hygromechanical material properties characterizations were conducted using TIM, underfill, laminates, and PCB materials individually soaked in 85°C/85RH according to Joint Electron Device Engineering Council (JEDEC) standard [14] by using thermal and humidity (T&H) chamber, balance and coordinate-measurement machine. From the measured weight gain and the dimensional change with time, moisture diffusivity D, saturated moisture concentration C_{sat}, as well as, coefficient of moisture expansion were determined for various materials within the package assembly. Using the measured D, moisture distribution with time within the package assembly was determined, assuming the package assembly to be dry at the start of the simulation.

That is, the initial condition was $w=0$ at all the nodes. During the 85°C/85RH soaking, $w=1$ and $\partial w/\partial n=0$ were applied at the boundaries. Symmetric structural boundary conditions were applied. For this model, Cu-lid, solder were assumed to have no moisture absorption. Once the moisture distribution was obtained, the moisture-induced mechanical stresses within the package assembly were determined using the coefficient of moisture expansion.

3 Model Validation

3.1 Thermal Mechanical Model Validation. The package deformation due to thermal excursions under dry conditions was validated using experimental data. The in-plane deformation contours were validated using laser Moiré while the out-of-plane warpage was validated using the data from an optical profilometer.

3.1.1 In-Plane Deformation Validation With Laser Moiré. A package assembly on a PCB was cross-sectioned along the centerline parallel to one of the edges. A 1200 lines/mm grating was adhered to the cross-sectioned surface of the sample using a high-temperature epoxy adhesive and the epoxy was cured at room temperature. The sample was then placed in the laser Moiré thermal chamber and the reference or null fringes were obtained at room temperature (23°C). The chamber was then heated to 85°C at a rate of 5°C per minute and was dwelled at 85°C for another

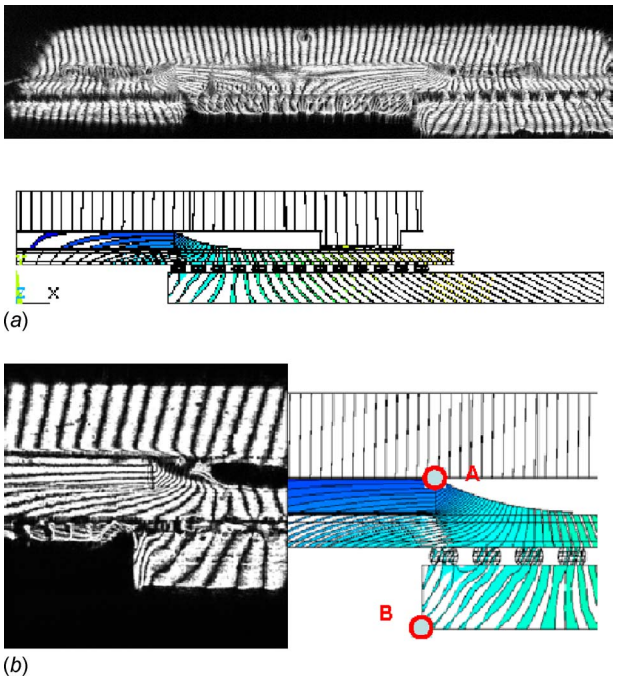

Fig. 6 (*a*) U_x displacement fringe comparison (overall) and (*b*) U_x displacement fringe comparison (chip edge)

15 min to ensure the whole sample would reach a steady-state temperature. U_x and U_y Moiré fringes were captured at 85°C. For additional details on laser Moire experiments, the reader is referred to Ref. [15]. Figures 6 and 7 show a comparison of laser Moiré images with finite-element contours. Figure 6(*a*) shows U_x contours for the entire package assembly while Fig. 6(*b*) shows the zoomed-in version of the contours near the chip edge. Similarly, Fig. 7 presents a comparison for U_y contours between laser Moiré experiments and finite-element simulations. As seen, the contours obtained through finite-element simulations are similar to the contours obtained through laser Moiré experiments. Differ-

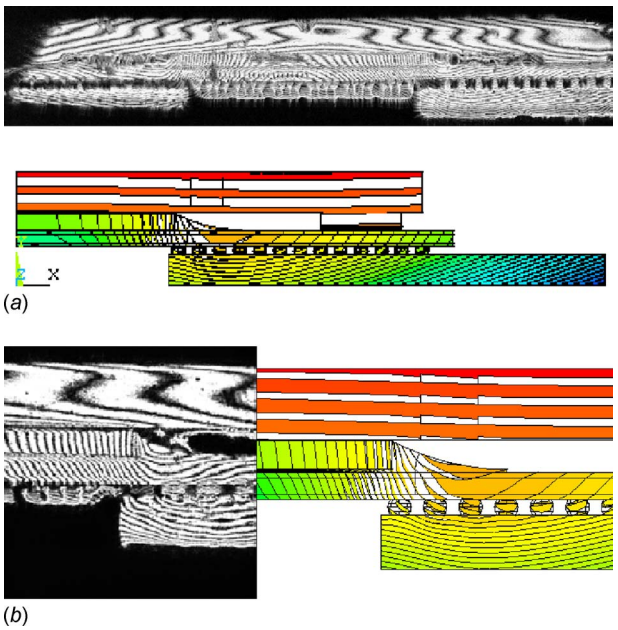

Fig. 7 (*a*) U_y displacement fringe comparison (overall) and (*b*) U_y displacement fringe comparison (chip corner)

Table 1 Comparison of warpage between optical profilometer measurement and FE analysis

Warpage	Profilometer (μm)	FEM (μm)	Error (%)
Chip	62	66.1	+6.6
Laminate bottom	172.4	171.5	−0.5

ential deformations from specific locations, such as chip edge (A) and board cut-out edge (B), were used to compare the results from finite-element simulations against experimental data and it was seen the finite-element simulations agree with the experimental data within 15%. Thus, Moiré experiments validate the finite-element simulations between loadstep 5 and loadstep 6, as illustrated in Fig. 5. However, the simulations assume the package assembly to be stress-free at loadstep 5 to mimic the null fringes for laser Moiré experiments for the package on board assembly at room temperature.

3.1.2 Out-of-Plane Warpage Validation With Optical Profilometer. In addition to in-plane deformation, the out-of-plane warpage deformation experimental data were obtained using an optical profilometer (Fries Research and Technology, Bergisch Gladbach, Germany). For this experiment, a flip chip reflowed on a laminates and an underfill (deck-level) was used to measure the warpage, which is similar to loadstep 1, as illustrated in Fig. 5. Table 1 presents a comparison between the warpage obtained through the optical profilometer and the finite-element simulations (Fig. 8) at two representative locations. As seen, the simulations agree with the experimental data within 6.6%

3.2 Hygromechanical Model Validation. As a first step in hygromechanical model validation, the moisture absorption was validated using weight gain data. Two module-level samples (after lid attach, loadstep 2) and six card-level samples were put in the 85°C/85RH chamber for 775 h to obtain the weight gain curve. Module-level samples consist of the chip, laminates with solder balls, underfill, TIM, copper lid, and sealband. The card-level sample consists of a module assembled on a PCB. The samples were taken out from the humidity chambers at regular intervals to measure the weight gain. In parallel to the moisture gain experiments, finite-element simulations were carried out using the wetness-temperature analogy, as explained earlier, for a module-level as well as a card-level mode. The moisture gains predicted from the models are compared against experimental moisture gain data, as illustrated in Figs. 9 and 10. As seen, moisture weight gain predictions from the finite-element models agree well with the experimental data.

The moisture weight gain curves, discussed above, validated the moisture diffusion part of this model. In order to calibrate the hygromechanical part, digital image correlation (DIC) warpage measurement was carried out before and after 775 h moisture soaking, following the standard measurement process in ARAMIS manual [16]. For this test, two module-level samples and six card-

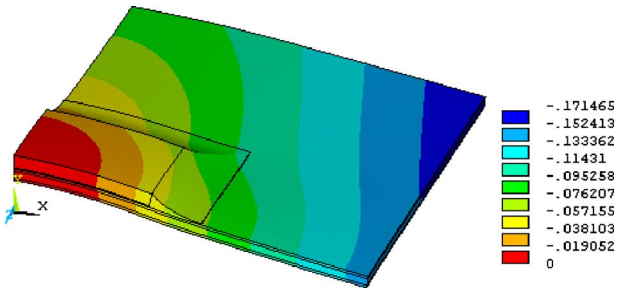

Fig. 8 Deck-level warpage (after underfilling, loadstep 1)

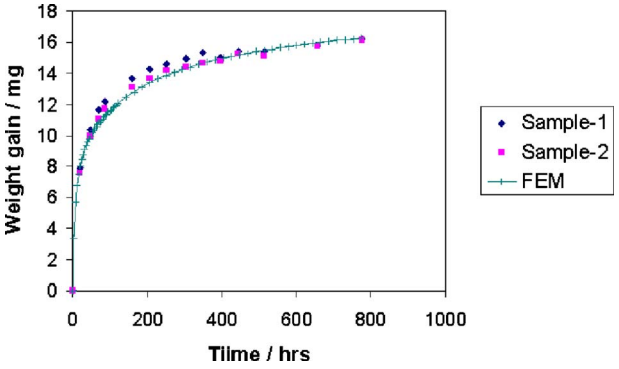

Fig. 9 Module-level moisture weight gain

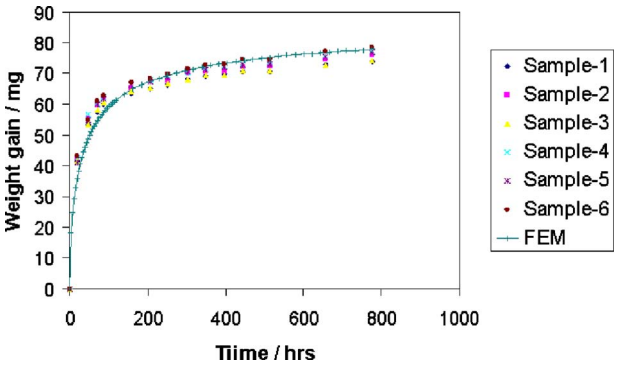

Fig. 10 Card-level moisture weight gain

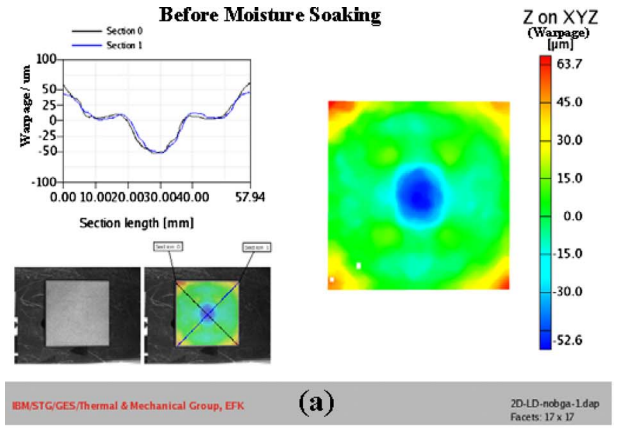

Fig. 11 Module-level, laminate bottom warpage (sample 1)

Table 2 DIC measurement of laminate warpage

Sample	Initial warpage (μm)	Warpage after soaking (μm)	Warpage due to moisture (μm)	Average warpage (μm)	Standard deviation
1	103.6	82.1	21.5	19.5	2.8
2	53.5	36.0	17.5		

level samples were used. The before-soaking as well as after-soaking measurements of these samples were carried out at room temperature. As all the measurements were conducted at room temperature, the measured warpage change is predominantly due to moisture soaking, not due to temperature changes. Figure 11 shows module-level laminate bottom warpage contours before and after moisture soaking and the center to corner warpage values at the bottom of the substrate for the module are presented in Table 2. Figure 12 shows the DIC contours before and after moisture soaking. As seen, the DIC contours are not symmetric about the diagonals. This nonsymmetry is due to different Cu trace patterns in the board and such trace patterns will influence the initial board warpage as well as the final board warpage after moisture absorption. Also, the nonuniform trace patterns will result in different amounts of moisture absorption in different quadrants of the PCB. Thus, the warpage was computed as the difference in the out-of-plane displacement of points A and B. Point A is at the corner of the board cutout and point B is at the board corner, as illustrated in Fig. 12(*a*). Four such measurements were done for the four corners of each board assembly and the average value for each board assembly is presented in Table 3.

Figure 13 shows the warpage contours of the module due to moisture absorption while Fig. 14 shows the warpage contours of the board assembly due to moisture absorption. The substrate warpage predicted by the model (Fig. 13) is around 20 μm and compares well with the experimental magnitude of about 19 μm, as given in Table 2. The board warpage predicted by the model (Fig. 14) is around 25 μm and has the same order of magnitude as the experimental data 14.5 μm, as given in Table 3. However, the values do not compare well due to the fact that the models assume planar isotropic behavior of the board for mechanical and hygroproperties.

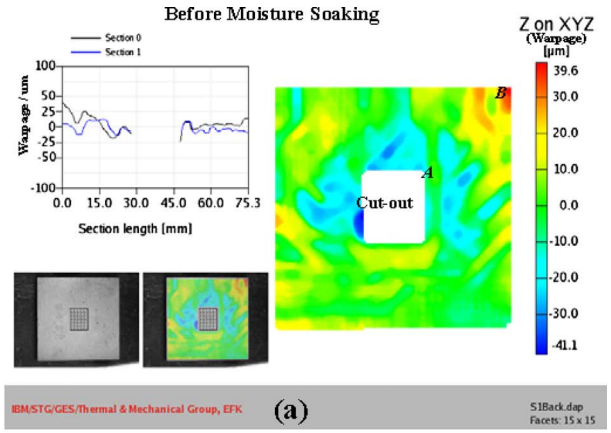

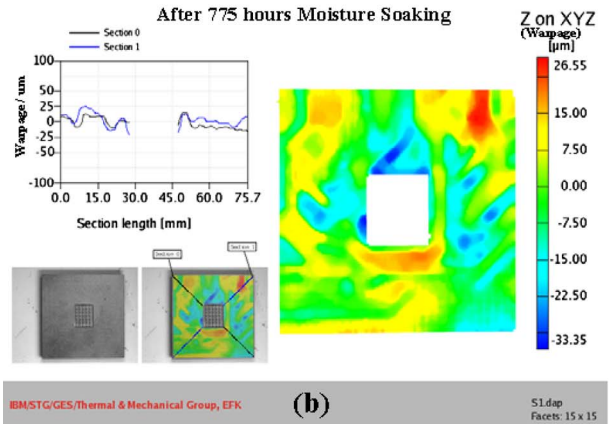

Fig. 12 Card-level, board bottom warpage (sample 1)

4 TIM Reliability

Having validated the thermomechanical and the hygromechanical models, the paper will now focus on the reliability of TIM using the developed models.

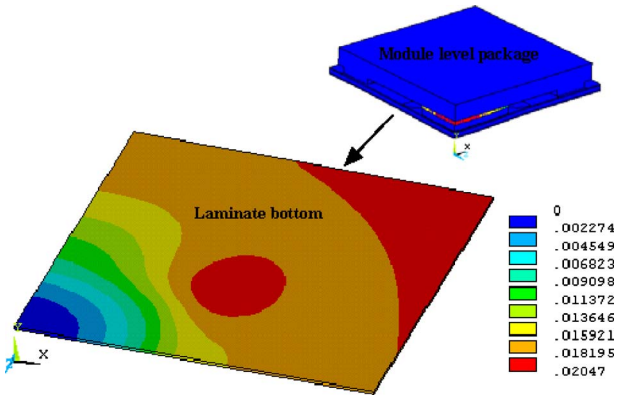

Fig. 13 Laminate bottom warpage (module-level)

Table 3 DIC measurement of board warpage

Sample	Initial warpage (μm)	Warpage after soaking (μm)	Warpage due to moisture (μm)	Average warpage (μm)	Standard deviation
1	29.1	21.1	8.0		
2	10.1	−2.9	13.0		
3	28.8	16.7	12.1		
4	25.4	8.3	17.1	14.6	4.3
5	−5.1	−23.4	18.3		
6	49.1	30.1	19.0		

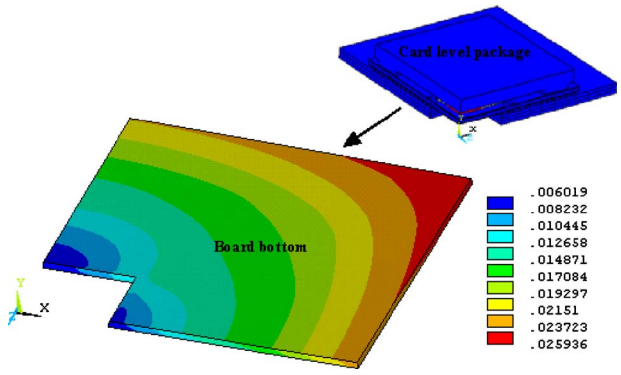

Fig. 14 Board bottom warpage (card-level)

4.1 TIM Strain During Assembly (Loadsteps 1–5). As illustrated in Fig. 8, the chip/laminates assembly warps down at room temperature in loadstep 1. This is due to the fact that the chip has a significantly lower coefficient of thermal expansion (CTE) compared with the laminates. Then the TIM and the sealband materials are dispensed and the lid is attached to the die through TIM and to the laminate through the sealband. The entire structure is then heated to loadstep 2 to cure the TIM and sealband. Following the curing, the structure is brought to room temperature as illustrated as loadstep 3 in Fig. 5. At loadstep 3, as in loadstep 1, the chip/laminates structure will warp down with a convex or dome shape compressing the TIM center and stretching the TIM corners. This will result in a compressive stress σ_y (and compressive strain ε_y) in the TIM center and a tensile stress σ_y (and tensile strain ε_y) at the TIM corner, as illustrated in Figs. 15(*a*) and 15(*b*). As seen in Fig. 15, the compressive stresses and strains are small in magnitude at the center while the tensile stresses and strains near the corner are large in magnitude, which may tear or debond TIM from the die and/or the lid. Thus, either the stress or the strain will be an appropriate metric to assess the propensity for TIM debonding. As TIM is a soft, pastelike material, TIM could break or debond from the chip or the Cu-lid. In the absence of any cohesive strength or interfacial adhesion strength measurements, either normal stress or strain can be used to understand TIM behavior under various loading conditions. Thus, for the purpose of studying the propensity for TIM delamination, we will use TIM strain in the thickness direction ε_y throughout this paper. Also, the use of normal strain facilitates easy addition of strain components for thermohygromechanical coupling purposes.

On the other hand, when the structure is subsequently heated to reflow temperature for BGA package assembly on a PCB, the chip/laminates assembly warps with a concave or a bowl shape resulting in a tensile strain at the TIM center and a compressive strain near the edges because of the high temperature during BGA reflow, chip warps as a concave shape, stretching the TIM center, and compressing the TIM corner, as illustrated in Fig. 16. The high magnitude of TIM strain at the center indicates that TIM may delaminate at loadstep 4 during reflow. However, after reflow and once it cools down to room temperature, ε_y at the TIM center becomes compressive while ε_y at the TIM corner becomes highly tensile (Fig. 17). Based on this thermomechanical study of the assembly process steps, one can conclude that TIM center delamination is concern at the high reflow temperature while TIM corner delamination is a concern near room or low temperatures.

4.2 TIM Strain After 500 h 85°C/85RH Soaking (Loadstep 7). Following the assembly process steps, when moisture soaking at 85°C/85RH is considered, the strains in the TIM continue to change with time, as illustrated in Fig. 18. As seen at loadstep 5, the normal strain at the TIM center is compressive while the normal strain at the TIM corner is tensile. As moisture is absorbed at 85°C, the strain in TIM continues to evolve with moisture absorption. Thus, TIM strain history curve (Fig. 18) indicates that both TIM center and corner strain increases during the 500 h soaking. And that TIM center and corner strains reach almost the same level after 500 h.

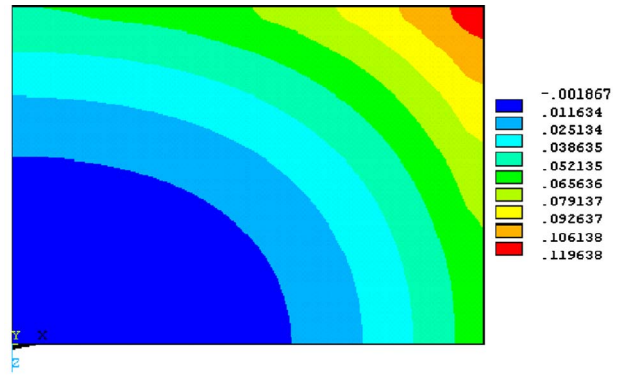

(*a*)

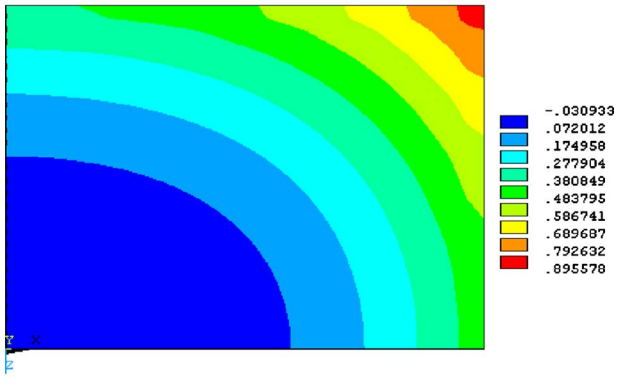

(*b*)

Fig. 15 (*a*) Stress σ_y in the TIM after lid attach and cool down to room temperature (loadstep 3) and (*b*) strain ε_y in the TIM after lid attach and cool down to room temperature (loadstep 3)

Figures 19(*a*) and 19(*b*) show the thermomechanical strain contours and the hygromechanical strain contours while Fig. 19(*c*) shows the combined thermohygromechanical strain contours at loadstep 7. As seen, the strain ε_y throughout TIM is tensile at loadstep 7 and this is a potential cause for concern for TIM delamination.

The ongoing research is currently examining various approaches to reduce the normal TIM strain and, thus, to reduce the chances for TIM delamination. Such approaches will be presented and discussed in a future publication.

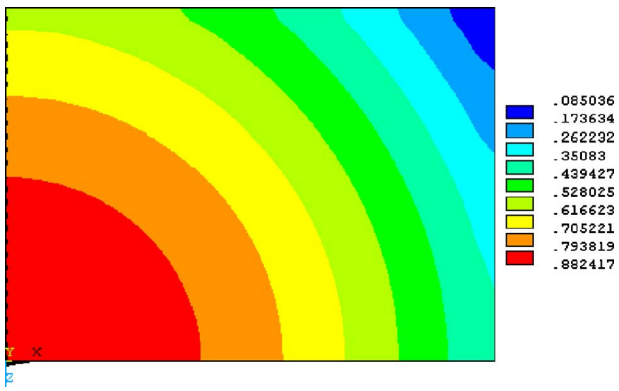

Fig. 16 Strain ε_y in the TIM at the reflow temperature (loadstep 4)

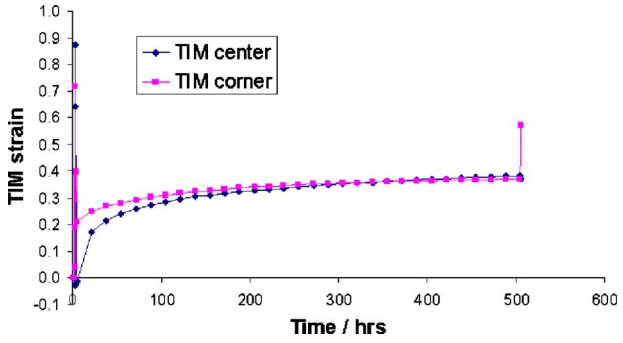

Fig. 18 TIM strain history during the whole process (loadstep 1 to 8)

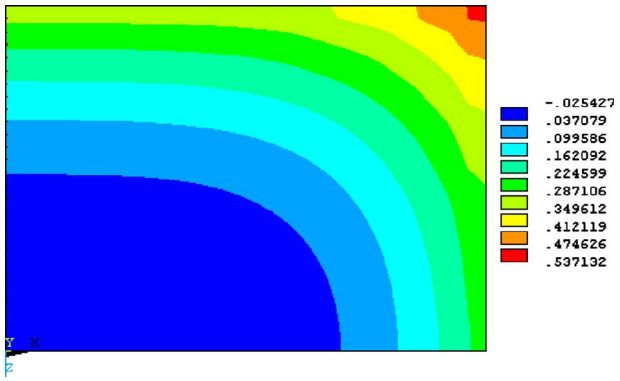

Fig. 17 Strain ε_y In the TIM at room temperature after reflow (loadstep 5)

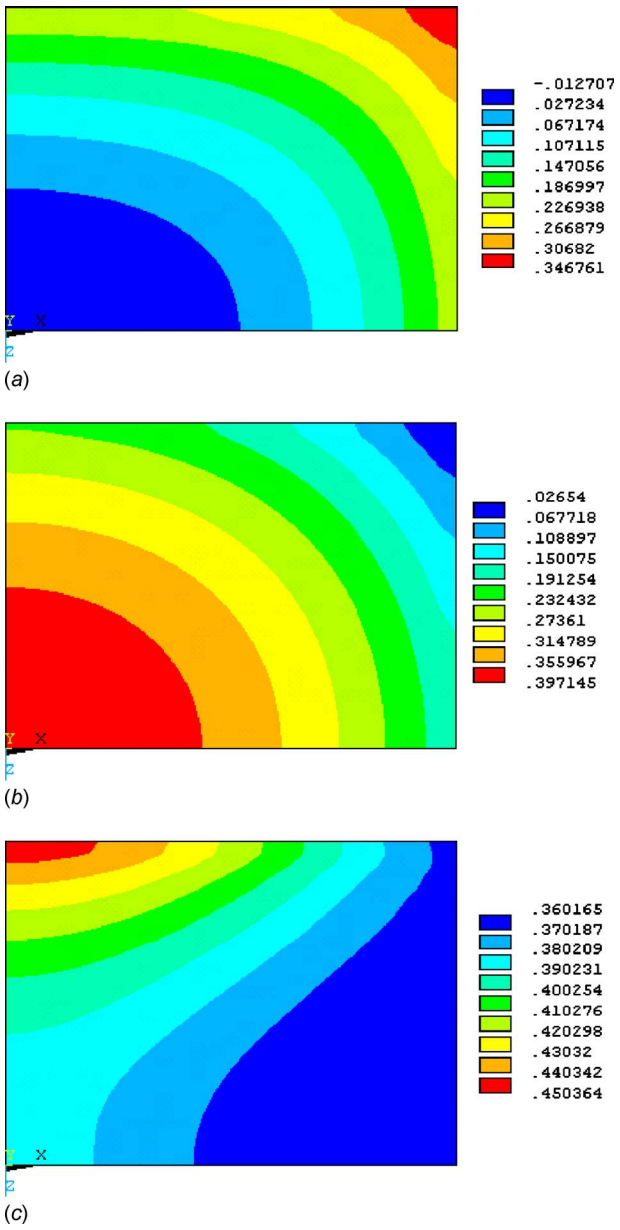

Fig. 19 (*a*) Thermal-mechanical strain ε_y in the TIM after 500 h 85°C/85RH soaking (loadstep 7), (*b*) hygromechanical strain ε_y in the TIM after 500 h 85°C/85RH soaking (loadstep 7), and (*c*) hygro-thermal-mechanical strain ε_y in the TIM after 500 h 85°C/85RH soaking (loadstep 7)

5 Summary

In this paper, a hygrothermal-mechanical sequential FE model was developed and validated with various experimental data. The developed model was used to study TIM reliability under thermo-mechanical modeling of assembly process steps as well as under hygro-thermo-mechanical modeling of 85°C/85RH soaking over 500 h. The models provide important insight into the potential for TIM delamination during package assembly and moisture soaking. It is seen that during reflow assembly of the package, TIM could potentially delaminate near the center. On the other hand, TIM could delaminate near the chip corner at room or lower temperatures. The magnitude of such thermomechanical strains is high and is a cause for concern for TIM delamination. When the package assembly is subsequently moisture soaked at 85°C/85RH over 500 h, tensile strains develop throughout the TIM material due to hygrothermal effects requiring alternate designs and/or process steps to reduce the high strains. Such approaches are currently pursued in our research.

Acknowledgment

The authors acknowledge IBM Corporation for the support of this work. The authors thank Mr. Pomerantz for FRT optical profilometer experimental data.

References

[1] Fukuzawa, I., Ishiguro, S., and Nanbu, S., 1985, "Moisture Resistance Degradation of plastic LSI's by Reflow Soldering," Proceedings of IRPS, pp. 192–197.
[2] Kitano, M., Nishimura, A., and Kawai, S., 1988, "Analysis of Package Cracking During Reflow Soldering Process," Proceedings of IRPS, pp. 90–95.
[3] Anjoh, I., Nishi, K., Kitano, M., and Yoshida, T., 1988, "Analysis of the Package Cracking Problem With Vapor Phase Reflow Soldering and Corrective Action," Soldering and Surface Mount Technology, **14**, pp. 48–51.
[4] Galloway, J. E., and Miles, B. M., 1996, "Moisture Absorption and Desorption Predictions for Plastic Ball Grid Array Packages," Proceedings of the Intersociety Conference on Thermal Phenomena, pp. 180–186.
[5] Tay, A. A. O., and Lin, T., 1996, "Moisture Diffusion and Heat Transfer in Plastic IC Packages," IEEE Trans. Compon., Packag. Manuf. Technol., Part A, **19**(2), pp. 186–193.
[6] Huang, Y. W., Teo, K. H., Chua, K. L., Yang, M. W. R., and Femg, W., 1999, "The Effects of Underfill on the Pressure Cooker Test Performance of Flip Chip on Board Assembly," Proceedings of InterPack, pp. 1121–1127.
[7] Wong, E. H., Rajoo, R., Koh, S. W., and Lim, T. B., 2002, "The Mechanics and Impact of Hygroscopic Swelling of Polymeric Materials in Electronic Packaging," J. Electron. Packag., **124**(2), pp. 122–126.
[8] Wong, E. H., Koh, S. W., Rajoo, R., and Lim, T. B., 2000, "Underfill Swelling and Temperature-Humidity Performance of Flipchip PBGA Package," Electronics Packaging Technology Conference, pp. 258–262.
[9] Stellrecht, E., Han, B., and Pecht, M. G., 2004, "Characterization of Hygroscopic Swelling Behavior of Mold Compounds and Plastic Packages," IEEE Trans. Compon. Packag. Technol., **27**(3), pp. 499–506.
[10] Ma, X., Jansen, K. M. B., Ernst, L. J., van Driel, W. D., van der Sluis, C. O., and Zhang, G. Q., 2007, "Characterization of Moisture Properties of Polymers for IC Packaging," Microelectron. Reliab., **47**(9–11), pp. 1685–1689.
[11] Cadge, D., Wang, H. J., Bie, J., Sun, X., and Gong, R. B. P., 2006, "Coupled

Thermal-Moisture-Stress Analysis for Electronic Packages," International Conference on Electronic Materials and Packaging, pp. 1–6.
[12] Fan, X., 2006, ECTC Professional Development Course.
[13] Wong, E. H., Chan, K. C., Lim, T. B., and Lam, T. F., 2000, "Non-Fickian Moisture Properties Characterization and Diffusivity Modeling for Electronic Packages," Electronics Packaging Technology Conference, pp 302–306.
[14] JESD22-A120A.
[15] Post, D., Han, B., and Ifju, P.,1997, High Sensitivity Moire: Experimental Analysis for Mechanics and Materials.
[16] ARAMIS User Manual.